

## Rossby Normal Modes in Basins with Barriers\*

JOSEPH PEDLOSKY AND MICHAEL SPALL

*Department of Physical Oceanography, Woods Hole Oceanographic Institution, Woods Hole, Massachusetts*

(Manuscript received 6 April 1998, in final form 22 October 1998)

### ABSTRACT

The Rossby wave, linear, normal modes for a barotropic fluid in a basin on the  $\beta$  plane are calculated in the presence of a thin barrier, which nearly divides the basin in two. Narrow gaps allow one subbasin to communicate to the other. In the case of a meridional barrier it is shown that the modes split into two categories: either full-basin modes, which have strong expression in both subbasins, or subbasin modes, which are limited to one or the other of the subbasins. The full-basin modes have natural frequencies very close to the eigenfrequencies of the basin in the absence of a barrier, while the subbasin modes oscillate at the eigenfrequencies of the subbasins as if they were isolated. In the former case, the oscillation is accompanied by strong flow through the gaps in the barrier while, in the latter case, there is essentially no flow through the barrier.

If the barrier is opened by adding additional gaps, some of the modes turn from subbasin modes to full-basin modes.

If the barrier is zonally oriented rather than meridionally oriented, the clear distinction between the two mode types disappears, although it is still possible to associate each of the modes with a subbasin mode restricted predominantly to one or the other of the subbasins.

The analytic theory, based on a narrow-gap assumption, is checked and extended by considering a linearized numerical model for the forced response of the basin. Of particular significance is the ability of localized forcing in one subbasin to excite oscillations of the full basin in spite of narrow gaps that restrict the communication between adjacent subbasins.

### 1. Introduction

The circulation of the deep ocean is strongly influenced by the presence of the midocean ridge system, which acts as an incomplete barrier to the deep circulation. The deep ocean is divided into subbasins by the presence of the ridge system, and the communication between the subbasins takes place largely through narrow gaps in the ridge offered by the faults in the ridge structure. In a recent paper, Pedlosky et al. (1997, hereafter PPSH) examined the steady circulation of a barotropic fluid in which an ocean basin is nearly divided in two by a meridional barrier, which allows communication between the two subbasins only through narrow gaps in the barrier that models the ridge. They found that the ridge was surprisingly ineffective in blocking the steady circulation between the two subbasins in spite of their near isolation. The degree of communication

between the two subbasins is measured by the value of the streamfunction on the ridge segment,  $\Psi_r$ , while the streamfunction is set to zero on the basin's outer boundary. The determination of  $\Psi_r$ , and so of the flux between the subbasins, follows from an application of the momentum circulation integral constraint around the "island" formed by the ridge segment.

As shown by Godfrey (1989), the original constraint can be replaced by a more convenient integral contour that encircles the island's western edge and proceeds along latitude circles to the eastern boundary. The linearized version of this constraint is called the "Island Rule," and one of the goals of the study of PPSH was to assess the robustness of this simplified rule when nonlinearity is important. In a barotropic model with no-slip conditions on all solid boundaries, it turns out that the relative vorticity fluxes, which could, in principle, alter the results of the island rule, were always very small. PPSH speculated that this result, which depends on the self-cancellation of the relative vorticity flux with no-slip conditions, would perhaps be modified in a baroclinic model where the eddy-thickness flux could contribute a non-self-canceling contribution to the potential vorticity flux. This encouraged us to examine a simple two-layer baroclinic numerical model in which the boundary layer flow on the eastern side of the ridge becomes baroclinically unstable, resulting in the devel-

\* Woods Hole Oceanographic Institution Contribution Number 9698.

*Corresponding author address:* Dr. Joseph Pedlosky, Department of Physical Oceanography, Woods Hole Oceanographic Institution, Woods Hole, MA 02543.  
E-mail: jpedlosky@whoi.edu

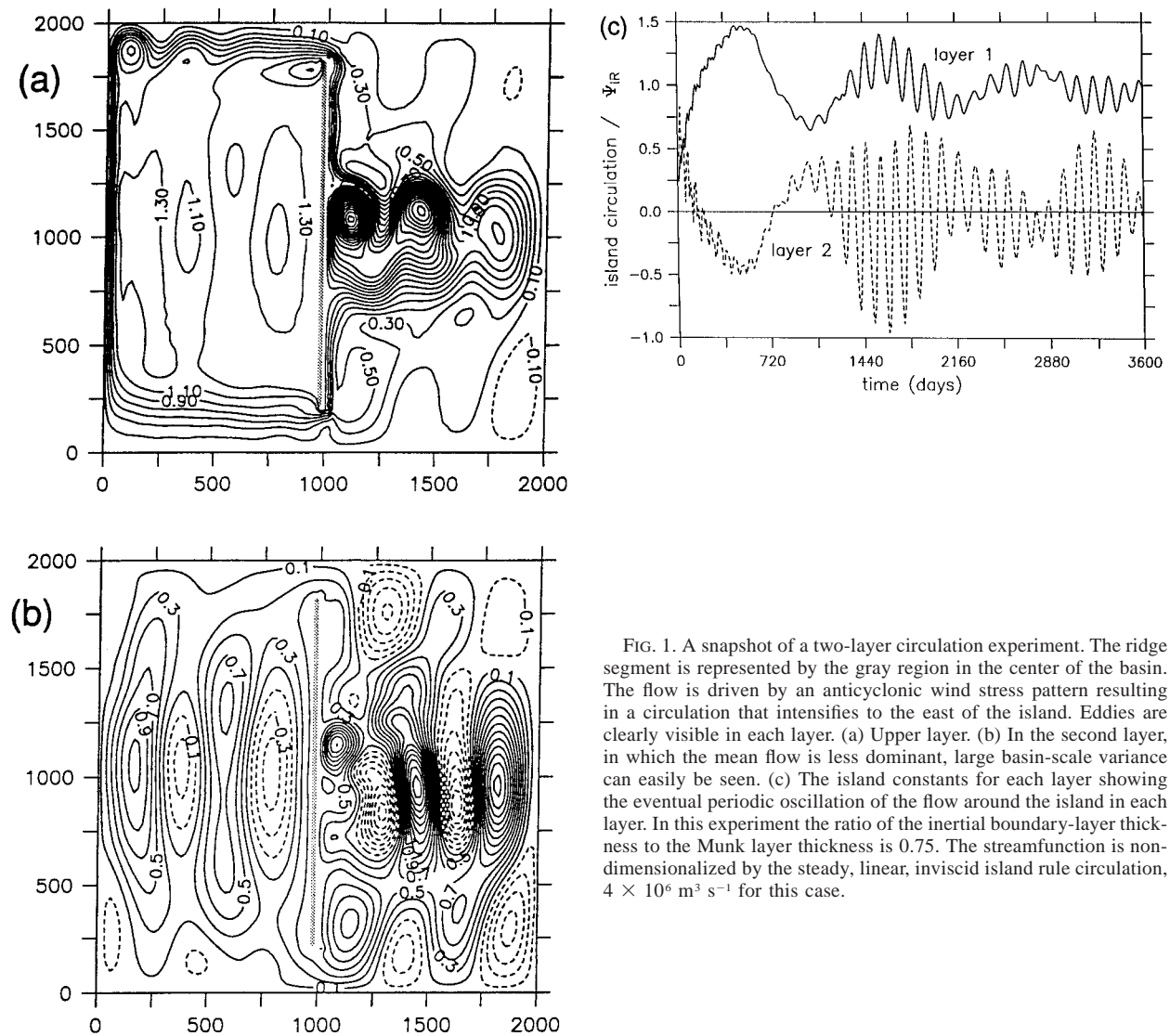


FIG. 1. A snapshot of a two-layer circulation experiment. The ridge segment is represented by the gray region in the center of the basin. The flow is driven by an anticyclonic wind stress pattern resulting in a circulation that intensifies to the east of the island. Eddies are clearly visible in each layer. (a) Upper layer. (b) In the second layer, in which the mean flow is less dominant, large basin-scale variance can easily be seen. (c) The island constants for each layer showing the eventual periodic oscillation of the flow around the island in each layer. In this experiment the ratio of the inertial boundary-layer thickness to the Munk layer thickness is 0.75. The streamfunction is nondimensionalized by the steady, linear, inviscid island rule circulation,  $4 \times 10^6 \text{ m}^3 \text{ s}^{-1}$  for this case.

oment, locally, of a set of deformation radius-scale eddies. Figure 1 shows a snapshot of the resulting flow in the two layers from one of our calculations. The flow is driven by an anticyclonic wind stress pattern, which results in a circulation of the type already described in PPSH. It intensifies on the eastern side of the island where a recirculation domain is formed. In the model, baroclinic instabilities of the boundary current give rise to a baroclinic eddy field. What we found particularly provocative in the preliminary calculations was the evidence, provided by the circulation pattern in layer two (where the mean flow is relatively weak), that the variance included structures evocative of basin-scale Rossby normal modes (Pedlosky 1987). Such structures have been found in our numerical calculations for both weakly and strongly nonlinear boundary layer flows. Note that in both Figs. 1a and 1b the activity on the eddy scale is restricted to the eastern subbasin while basin-

scale disturbances, especially clear in the lower layer, exist in both subbasins and have full meridional basin extent. Figure 1c shows the time history of the streamfunction on the island in each layer. After an initial adjustment period of about 1200 days these (spatial) constants settle into a periodic oscillation whose periods are roughly consistent with estimates, not given here, of basin-scale normal modes for the baroclinic model. The question that then intrigued us was how it was possible to excite basin-scale normal modes in a situation where the forcing, in this case the eddy field, tends to be concentrated in one of the two subbasins so nearly isolated from the other. That is, are there such full-basin normal modes even when the two subbasins are nearly isolated from one another and can communicate only through very narrow gaps?

It seemed to us that the first question to address is the nature of the Rossby normal modes in a basin nearly

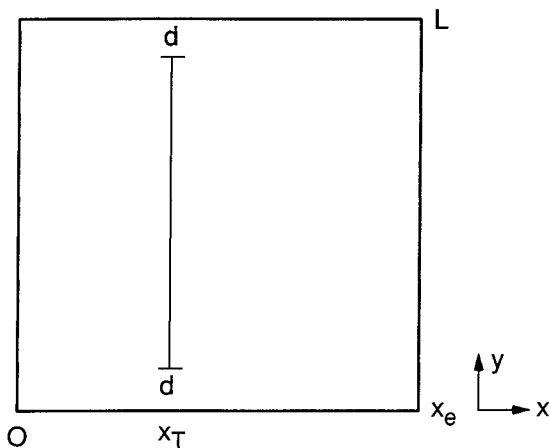


FIG. 2. A schematic of the full basin with a thin ridge nearly separating the basin into two. Small gaps of width  $d \ll L$  allow communication between the two subbasins. The ridge is located at  $x = x_T$ . The zonal width of the basin is  $x_e$  and its meridional extent is  $L$ .

bifurcated by a narrow ridge system with only narrow gaps providing routes of communication between the subbasins. Our preliminary intuitive notion was that the Rossby normal modes in a basin such as that depicted in Fig. 2, where  $d \ll L$ , would to the first approximation be represented by the union of the two sets of the normal modes for each subbasin, taken separately, with perhaps a small “leakage” of energy to the other basin.

However, the circulation integral constraint around each island (see section 2) disallows such a simplistic picture and, indeed, it follows that the set of normal modes falls instead into two categories. One type of mode is a full-basin mode in which each side of the basin oscillates in synchrony. The other is, as expected, limited to one or another of the subbasins. Which one occurs depends on the meridional structure of the mode and its ability to satisfy the circulation integral condition without involving the other subbasin. We believe it is significant that the gravest mode in the system turns out to be a full-basin mode, easily excited by localized forcing in one of the subbasins. The important implication is that local time dependence, produced by local process, can still involve the whole basin in time-dependent fluctuations even in the presence of extensive topographic barriers in the basin that might be expected to shield parts of the basin from regions of forcing. While pure basin normal modes may never be observed in the natural ocean, they are the building blocks with which basin-scale variability can be efficiently described. Although we have focused on the structure of the normal modes in the basin, the reader will appreciate that the more fundamental question addressed is the possibility of the transmission of energy through the narrow gaps from one subbasin to the next, which is more general than the normal mode problem.

In section 2 we formulate the mathematical problem

for the Rossby normal modes. The integral condition is derived and its implications for the mode problem are clarified. For the case of the geometry in Fig. 2, an analytical approach is developed for the normal-mode problem, and the dispersion relation and the eigenfunctions are found. In section 3 the problem is somewhat generalized by considering the modifications that occur when a gap is opened in the middle of the ridge/barrier, which serves to illuminate the fundamental role of gaps in providing basin-scale modes.

In section 4 we discuss the problem in which the ridge is oriented in a purely zonal direction, which introduces some new features to the normal mode problem.

Results of a linear numerical model of the *forced* response of the basin are included for each of the problems outlined above. This is done to illustrate the ability of local forcing to excite global modes in the nearly bifurcated basin and serves as a useful check on the analytic theory, which involves some approximations based on the smallness of  $d/L$  and which are not required by the numerical calculation.

Section 5 summarizes our results and discusses the implication for the general circulation problem and outlines the direction of future research.

## 2. Formulation: Single ridge

We consider the small-amplitude, nondissipative free modes of motion in a basin configured as in Fig. 2. For simplicity the widths of the northern and southern gaps,  $d$ , are taken equal. It is important to note that the barrier, which is our simple model of a midocean ridge, is placed at an arbitrary longitude in the basin. In particular, the ratio of the zonal extents of each subbasin is not the ratio of integers. This is done to guard against the possibility that a normal mode with a frequency appropriate for one subbasin would “accidentally” excite its neighbor and so disguise itself as a full-basin mode. In this study we examine the simplest case of a barotropic fluid.

The eigenvalue problem for the normal modes has some special aspects of interest. The presence of the detached barrier renders the region of the flow multiply connected. For each such segment a new condition, the conservation of circulation around the island, must be satisfied. Each condition is accompanied by an unknown constant value of the streamfunction on the segment. It is important to recognize that, since each constant is accompanied by an additional integral constraint, the overall normal mode problem remains homogeneous. A similar, but distinct, constraint arises for the normal modes of a baroclinic fluid or a barotropic flow with a free surface where the nontrivial value of the streamfunction on the rim of the basin is required to satisfy mass conservation (see Flierl 1977; Pedlosky 1987).

### a. Theory

The governing equation of motion is assumed to be the linear, quasigeostrophic potential vorticity equation on the  $\beta$  plane (Pedlosky 1987)

$$\frac{\partial \nabla^2 \psi}{\partial t} + \beta \frac{\partial \psi}{\partial x} = 0, \tag{2.1}$$

where  $\psi$  is the geostrophic streamfunction and the other variables have their standard definitions. The basin is taken to be rectangular. Its north–south extent is  $L$  and its east–west extent is  $x_e$ . The barrier is placed at  $x = x_t$  and fails to completely separate the basin into two independent parts only because of the presence of two gaps at the terminal extremes of the barrier. The gaps each have width  $d \ll L$ .

On the perimeter of the basin  $\psi$  must be constant and we can consistently choose that constant to be zero. On the barrier  $\psi$  will be some other (spatial) constant.

We look for free solutions of (2.1) in the form

$$\psi = e^{i(\omega t + k(x - x_t))} \phi(x, y), \tag{2.2}$$

which leads to the Helmholtz equation for  $\phi$ ; that is,

$$\nabla^2 \phi + k^2 \phi = 0, \tag{2.3}$$

if we choose  $k = \beta/(2\omega)$ . In (2.2) and in similar subsequent formulas, the real part of the complex expression is assumed.

On the barrier, the streamfunction is given by

$$\psi = \Psi_t e^{i\omega t} \tag{2.4}$$

so that on each side of the ridge (whose finite thickness is ignored)

$$\phi = \Psi_t, \quad x = x_t. \tag{2.5}$$

It is useful to rewrite the problem in nondimensional variables. If we choose  $L$  as the length scale and  $\beta L$  as the scale for the frequency, the governing equation remains (2.3) but where now all variables are nondimensional and where now  $k = 1/(2\omega)$ . The range in  $y$  becomes  $(0, 1)$  while  $x_e$  and  $x_t$  refer to their scaled, nondimensional values. Since  $\phi$  vanishes at  $y = 0$  and  $1$ , it is useful to represent the solution as a sine series in  $y$ . Further, it is convenient to express the solution separately in each subbasin. It follows that the solution on the left- and righthand subbasins can be written:

$$\begin{aligned} \phi_L &= \sum_{n=1} B_n \frac{\sin a_n x}{\sin a_n x_t} \sin(n\pi y) \\ \phi_R &= \sum_{n=1} A_n \frac{\sin a_n (x - x_e)}{\sin(a_n x_{te})} \sin(n\pi y), \end{aligned} \tag{2.6}$$

where

$$a_n = [k^2 - n^2 \pi^2]^{1/2} \quad x_{te} = x_t - x_e. \tag{2.7}$$

At  $x = x_t$  the streamfunction, and hence  $\phi$  must be equal to  $\Psi_t$ , on the barrier. At the same time the streamfunction must fall to zero at  $y = 0$  and  $y = 1$ . We assume that for  $d$  (here scaled by  $L$ )  $\ll 1$ , it is sufficient to represent the streamfunction over the whole range of  $y$  approximately as

$$\psi = \Psi_t \begin{cases} y/d, & 0 \leq y \leq d \\ 1, & d \leq y \leq 1 - d \\ (1 - y)/d, & 1 - d \leq y \leq 1. \end{cases} \tag{2.8}$$

This implicitly assumes that the scale of the motion is generally greater than the scale of the gap,  $d$ , so that flow through the gap is smooth and unidirectional within the gap. Other, simple forms for the profile of flow through the gap yielded similar results. If (2.8) is applied to (2.6) it follows that

$$A_n = B_n = -2\Psi_t [(-1)^n - 1] \frac{\sin n\pi d}{n^2 \pi^2 d}. \tag{2.9}$$

Note that this implies that  $A_n$  and  $B_n$  would be zero for even values of  $n$ , yielding a zero contribution to the streamfunction unless one of the denominator terms in (2.6) was zero. This condition is equivalent to the condition that one of the subbasins is in resonance with an even  $n$  mode. Even  $n$  modes correspond to streamfunctions that are odd around  $y = 1/2$ , so such normal modes must be limited, if they exist, to one or another of the subbasins. Since the flow through the two narrow gaps must be equal and opposite in barotropic, quasigeostrophic theory (since there is no mass storage on either side of the basin), the even  $n$  modes have the wrong symmetry for interbasin communication.

The final condition determining the dispersion relation for the modes is the integral condition on the circulation around the ridge. As PPSH show, in the absence of forcing, nonlinearity, and dissipation the integral constraint reduces to the conservation of circulation; that is,

$$\frac{\partial}{\partial t} \oint_{C_t} \mathbf{u} \cdot d\mathbf{s} = 0, \tag{2.10}$$

where  $C_t$  is the contour encircling the ridge. For any infinitesimally thin ridge (2.10) becomes

$$\int_d^{1-d} v(x_{t+}, y) dy = \int_d^{1-d} v(x_{t-}, y) dy. \tag{2.11}$$

Here  $x_{t+}$  and  $x_{t-}$  refer to the position of either side of the ridge and where  $v$  is the meridional velocity. Application of (2.11) to the solution given by (2.2), (2.6), and (2.9) yields the final dispersion relation:

$$\Psi_t \sum_{n=1} [(-1)^n - 1]^2 \frac{\sin 2n\pi d}{n^3 \pi^3 d} a_n \frac{\sin a_n x_e}{\sin a_n x_t \sin a_n x_{te}} = 0. \tag{2.12}$$

Note that the dispersion relation only involves Fourier modes for which  $n$  is odd. These are the modes that possess a nonzero average value of meridional velocity along each side of the ridge. On the other hand, the modes composed of sine functions with  $n$  even trivially satisfy (2.11) and are not governed by (2.12). Thus the

TABLE 1. Frequencies of the full-basin modes. The frequency of the four largest frequencies  $\omega$  of the normal modes for the case  $x_i = (0.15)^{1/2}$  and  $d = 0.1$ . Corresponding to each frequency is the normal-mode frequency,  $\hat{\omega}$ , for the same full basin in the *absence* of the barrier.

$\omega$	$(m)$	$\hat{\omega}$
0.1089	1	0.1125
0.0708	2	0.0712
0.0504	3	0.0503
0.0384	4	0.0386

total set of eigenvalues comprise two subsets. First, solutions of either

$$\sin a_n x_i = 0 \quad (2.13a)$$

or

$$\sin a_n x_{ie} = 0 \quad (2.13b)$$

for  $n$  even correspond to subbasin modes. For example, modes limited to the lefthand subbasin have normal-mode frequencies:

$$\omega_{nm} = \frac{1}{2\pi[n^2 + (m/x_i)^2]} \quad (2.14a)$$

for which

$$\phi_L = \sin(m\pi x/x_i) \sin n\pi y, \quad \phi_R = 0, \quad (2.14b)$$

and  $n = 2, 4, 6, \dots$

While another set of modes limited to the righthand subbasin is given by

$$\omega_{nm} = \frac{1}{2\pi(n^2 + (m/x_{ie})^2)} \quad (2.15a)$$

and

$$\phi_R = \sin(m\pi x/x_{ie}) \sin n\pi y \quad \phi_L = 0, \quad (2.15b)$$

also for  $n = 2, 4, 6, \dots$ , for integral  $m$ .

These modes correspond to  $\Psi_l = 0$  and hence to no mass transfer through the gaps. These normal modes are limited to one of the subbasins with no expression in the neighboring subbasin. Modes with the alternative meridional symmetry, for example, *symmetric* around the midlatitude of the basin must involve both subbasins in order to satisfy the circulation condition (2.11). For these modes, to which only odd  $n$  contribute, the dispersion relation is given by (2.12). These are the full-basin modes. The subbasin modes given by (2.14) and (2.15) are identical to the normal modes of a basin without topography and are well known (Pedlosky 1987). Therefore, we concentrate our discussion on the full-basin modes.

The solution of the dispersion relation (2.12) is easily obtained numerically. In Table 1 the first four (highest) frequencies are given as obtained from (2.12). Along with these frequencies are listed the normal-mode frequencies for a given  $x$ -modal wavenumber  $m$  each for the  $y$ -modal wavenumber  $n = 1$ , that is, for  $\phi =$

$\sin(m\pi x/x_e) \sin n\pi y$ . It is remarkable how close the two frequencies are to one another. It appears that the meridional barrier is surprisingly ineffective in altering the basic mode of oscillation of the basin.

The corresponding eigenfunctions for  $\phi$  are shown in Fig. 3. We call these functions the membrane functions since they are solutions of the Helmholtz equation (2.3). This function must be multiplied by the traveling wave factor as given by (2.2) to obtain the complete solution. Note that the square of the membrane function yields, for the meridional barrier, the distribution of mean-squared variance in the model.

Figure 3a shows the membrane function corresponding to the spatially gravest mode. Its frequency, as we see from Table 1, is very close to the  $m = 1, n = 1$  mode of the classical problem without the barrier and, indeed, the overall structure is reminiscent of the  $m = 1$  mode. There are distinctive differences, especially in the vicinity of the barrier. A large closed cell in  $\phi$  exists to the east of the barrier. The crowded streamlines at the gaps indicate the rush of fluid from one subbasin to the next during the oscillation. Figures 3b and 3c show the modes that correspond to the  $n = 1, m = 2$ , and  $m = 3$  modes of the classical, barrier-free problem and the qualitative correspondence to those wavenumbers is obvious. Figure 3d presents a qualitatively interesting change. The frequency of this mode is very close, as Table 1 shows, to the no-barrier mode  $m = 4, n = 1$ . The eigenfunction shows a considerable presence of the  $n = 3$  Fourier mode in  $y$ . Indeed, the structure of this mode is rather complex consisting of one cell to the east of the ridge, which appears to be a banana-shaped  $n = 1$  mode, while to the west of the ridge an  $n = 3$  structure is apparent. There is no particular significance to east and west determining this modal structure. If the barrier were moved to the mirror point  $x_i \approx 0.6217$ , the same structure would appear but reflected around the barrier. Of course the complete streamfunction consists of the product of the membrane function and the appropriate traveling wave whose wavenumber  $k = 1/(2\omega)$ . Figure 4 shows the fourth mode at four stages of the cycle showing the composite character of fixed modal shape and traveling wave.

Quite clearly, the presence of the barrier has a profound effect on the structure of the modes although the frequencies of the oscillations remain close to the barrier-free case. Calculations, not shown here, demonstrate only a slight variation in the normal-mode frequencies as the gap width  $d$  decreases. If  $d = 0.02$ , for example, the gravest-mode frequency falls to 0.091. For the higher  $m$  modes the effect is slighter.

We emphasize that in addition to the modes shown in Figs. 3 and 4, there are the subbasin-scale modes restricted to one or the other of the two subbasins. The amplitude of the oscillation is zero in the other subbasin. Their frequencies are given by (2.14a) and (2.15a). For the same value of  $x_i$  and  $d$  as in Table 1, these subbasin mode frequencies are given in Table 2. The modal

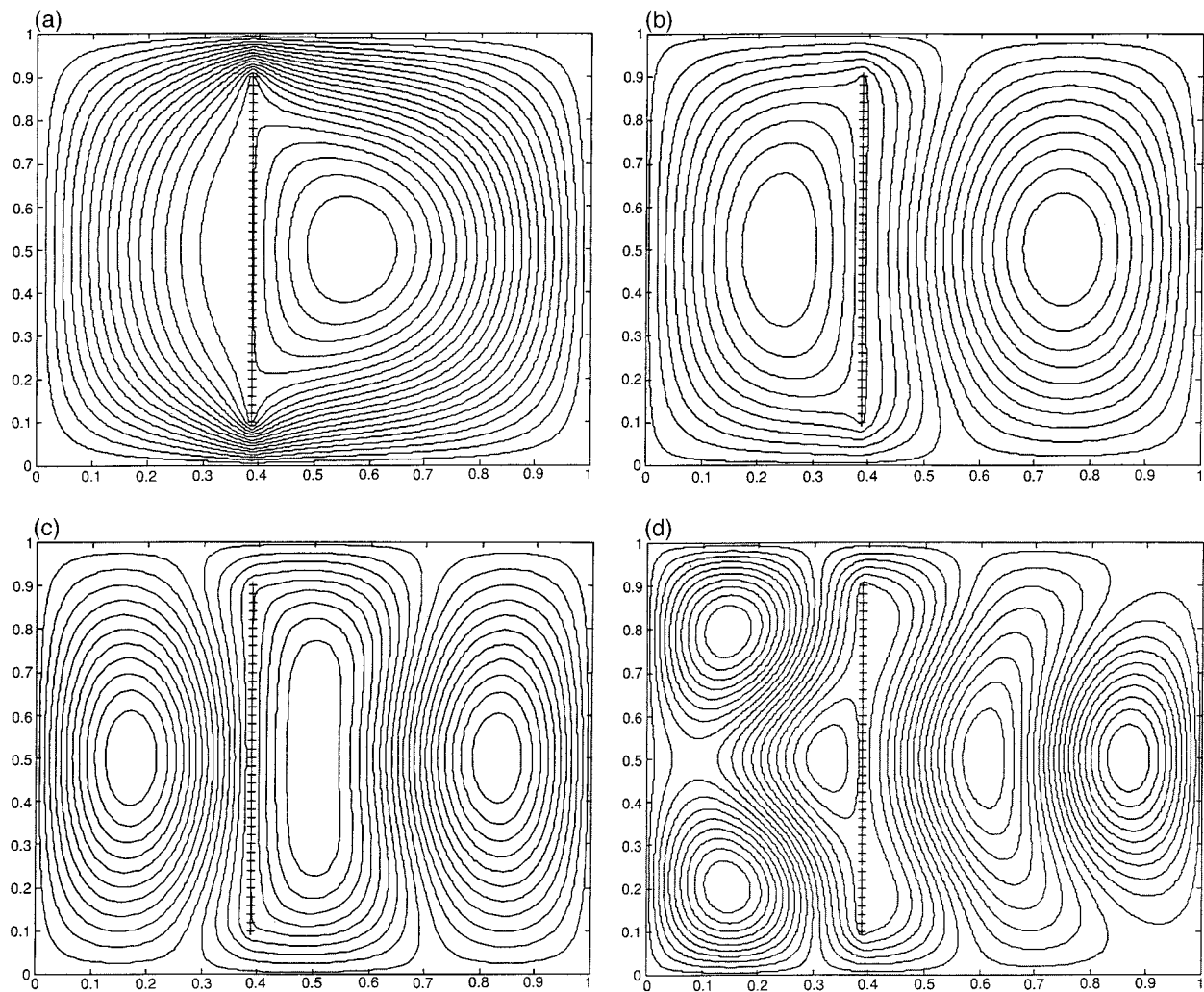


FIG. 3. The membrane function  $\phi$  for the first four eigenmodes in the presence of a meridional barrier at  $x = x_c = (0.15)^{1/2} \approx 0.387$  for  $d = 0.1$ . In this case,  $x_c = 1$ . (a) The gravest mode ( $m = 1$ ), (b) the second mode ( $m = 2$ ), (c) the third mode ( $m = 3$ ), and (d) the fourth mode ( $m = 4$ ). The index  $m$  corresponds to the mode of the basin without the barrier closest to the normal-mode frequency obtained from (2.12).

shapes are given by (2.14b) and (2.15b) and are not shown.

*b. Numerical model results*

The numerical model used in this study is based on the Miami Isopycnal Coordinate Ocean Model (MICOM) documented by Bleck et al. (1992). Only a brief summary of the model is included here, the model equations are given in appendix B, and details of the solution procedure and model configuration can be found in Bleck et al. (1992) and PPSH. A number of simplifying assumptions have been made for the present study. The temperature and salinity are constant within each isopycnal layer, so the model effectively carries only the potential density field. There is only one active layer so that the pressure gradient is due only to variations in

the surface elevation. The model has been made adiabatic by turning off the diapycnal mixing and surface buoyancy forcing. The only forcing in the system is a body force parameterization of a surface or interfacial stress. The nonlinear terms in the momentum equations have been set to zero, so all calculations presented in the remainder of the paper are linear (the model calculation in Fig. 1 contains the nonlinear terms). There is no explicit viscosity or thickness diffusion in the model. Because the model solves for the free surface height there is no need to independently specify the pressure on the island, as is required for models that make the rigid-lid approximation.

The model is configured in a square basin of width  $L = 2000$  km with a flat bottom at 16 000-m depth. The Coriolis parameter varies linearly with latitude as  $f(y) = f_0 + \beta y$ , where  $f_0 = 0.5 \times 10^{-4} \text{ s}^{-1}$  and  $\beta = 2 \times$

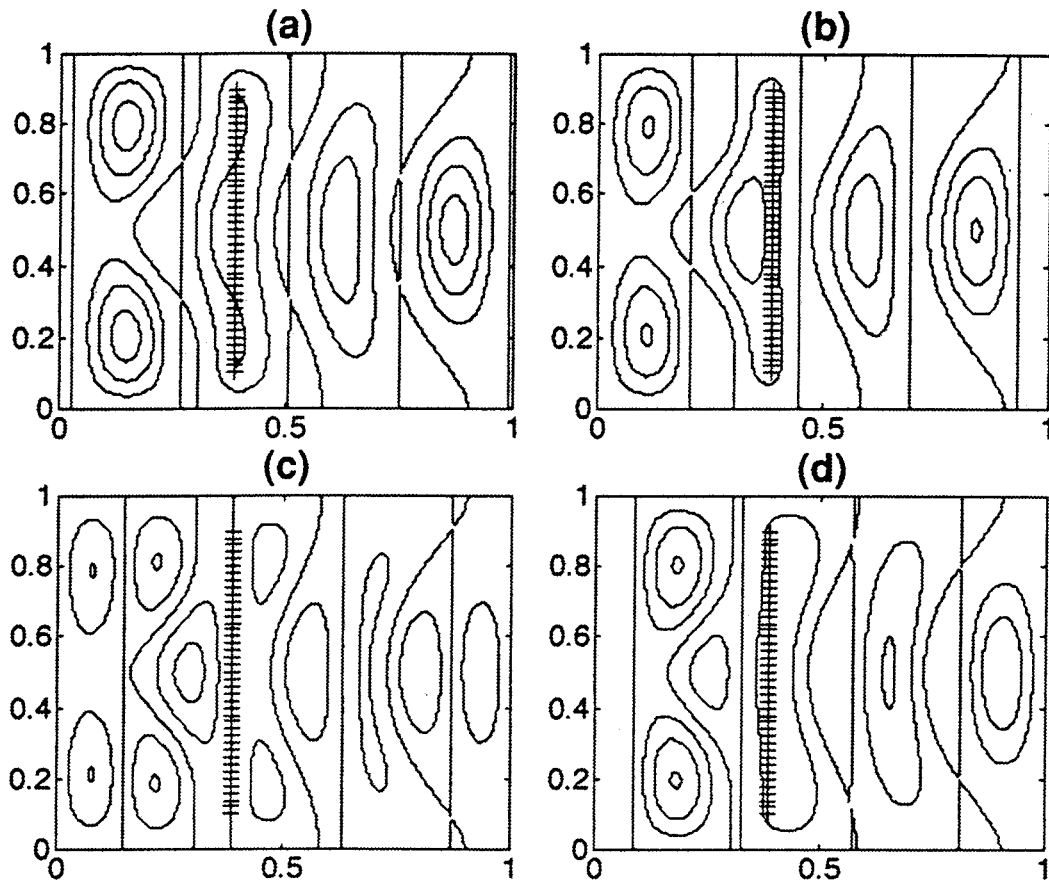


FIG. 4. Mode 4, corresponding to the membrane function of Fig. 3d at phases (a) 0, (b)  $\pi/4$ , (c)  $\pi/2$ , and (d)  $3\pi/2$ .

$10^{-13} \text{ cm}^{-1} \text{ s}^{-1}$ . The deformation radius at the middle of the basin is approximately  $R_d = 5.7 \times 10^9 \text{ cm}$ , giving  $L/R_d = 0.035$ . Smaller values of  $R_d$  shift the resonance of the basin modes to lower frequency; however, the results are qualitatively unchanged. We have sought to make  $L/R_d$  as small as possible by choosing an artificially large depth (within computational constraints) in order to make a quantitative comparison with the barotropic theory in the preceding section. The island is one grid point wide and located at 780 km from the western boundary. The gaps at the northern and southern ends of the island are 200 km wide. These values correspond to the previously defined nondimensional variables  $x_i = 0.39$  and  $d = 0.1$ . The model is forced with an oscillatory wind stress between 1500-km and 2000-km longitude. The meridional distribution of the wind stress is given by

$$\tau(y) = \begin{cases} 1, & y < y_s \\ \frac{1}{2} \left[ 1 + \cos \left\{ \frac{\pi(y - y_s)}{(y_n - y_s)} \right\} \right], & y_s < y < y_n \\ 0, & y > y_n. \end{cases} \quad (2.16)$$

The wind stress curl is confined between latitudes  $y_s = 700 \text{ km}$  and  $y_n = 1300 \text{ km}$  and is thus symmetric about the midlatitude of the basin.

A series of forced numerical calculations was carried out in which the frequency of the wind forcing (nondimensionalized by  $\beta L$ ) was varied from  $\omega = 0.03$  to  $\omega = 0.12$ . Resonant basin modes are indicated by peaks in the amplitude of the streamfunction variance evident in Fig. 5. The width of the peak is controlled by the duration of the calculations (500 days) because, while the resonant response continues to grow linearly in time, the amplitude of the response at off-resonant frequencies equilibrates at some lower amplitude. The frequency of the model resonances correspond to the theoretical frequencies for the  $n = 1$  modes discussed in the previous section. The frequency of the gravest mode in the model is 4% lower than the theoretical frequency, while the

TABLE 2. The four highest frequencies of the subbasin modes.

$\omega$	(m)	(n)	Subbasin
0.061 65	1	2	Right
0.048 73	1	2	Left
0.041 57	2	2	Right
0.028 74	2	2	Left

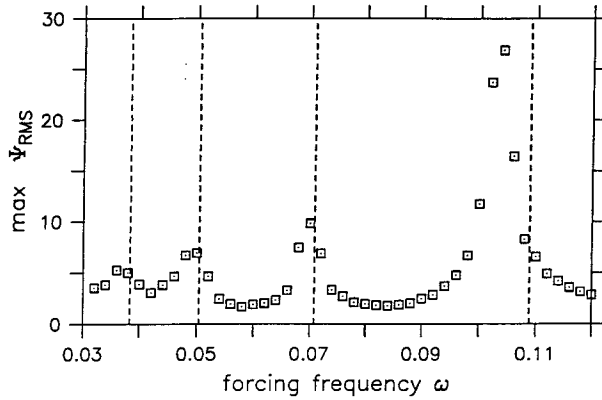


FIG. 5. Maximum variance of the modeled streamfunction within the basin as a function of forcing frequency (500-day integration time). Dashed lines indicate theoretical frequencies of the  $n = 1, m = 1, 2, 3,$  and  $4$  modes. The streamfunction has been nondimensionalized by the transport around the island expected from the linear island rule if the wind forcing were held constant in time.

frequencies at the  $m = 2$  and  $m = 3$  modes are within 1%, and the  $m = 4$  mode is within 5% of the theoretical result. The  $m = 2, n = 2$  and  $m = 1, n = 2$  modes of the right subbasin are not excited, even though they have resonant frequencies within the forcing frequencies, because the forcing is symmetric about the midlatitude of the basin. This forcing was chosen in order to isolate, as much as possible, the  $n = 1$  modes discussed in section 2a.

The spatial structure of the modes is indicated in Fig. 6. The  $m = 1$  and  $m = 2$  modes compare very closely with the theoretical result. The  $m = 3$  mode at  $\omega = 0.05$  has a similar structure to the theoretical result in the zonal direction, but the eastern subbasin also contains some higher-order structure in the meridional direction. It is likely that the  $n = 3, m = 1$  mode of the eastern subbasin has been partially excited by the oscillatory forcing as its resonance lies close in frequency space at  $\omega = 0.0466$ . The structure of the peak at  $\omega = 0.036$  (corresponding to the  $m = 4$  mode) reflects elements of the theoretical structure, including the  $m = 4$  zonal structure and the higher-order meridional structure in the western basin. However, there is also a strong element of an  $n = 3$  mode in the eastern subbasin, probably a signature of the  $n = 3, m = 2$  mode of the eastern subbasin, which has frequency 0.0358.

These results demonstrate that the theoretical basin-scale modes derived above can be excited by localized forcing in one of the subbasins. Resonant responses are found in the model for forcing near the theoretical frequencies of the basin modes, while smaller amplitude responses with a horizontal structure determined by a superposition of near-resonant modes are found at intermediate frequencies. The structure of the flow through the gaps found in the model is nearly linear for these cases (not shown), validating the assumption of a

linear streamfunction profile across the gaps that was used to close the theory.

The results also suggest that the oscillatory behavior found in the two-layer, wind-driven calculation shown in Fig. 1 is the signature of a similar basin-scale normal mode in which the western subbasin is excited by flow through the narrow gaps at the northern and southern tips of the island. The higher mode structure to the east of the island is probably a signature of an  $n = 3$  eastern subbasin mode that has frequency similar to the  $n = 1$  basin-scale mode.

### 3. Two ridge segments

Figure 7 shows a situation in which the ridge is pierced by another gap midway along its length. To simplify the resulting algebra and to make the results more immediately understandable, we have chosen a case in which the middle gap is precisely halfway along the ridge between its termini and we have chosen the northern and southern gaps to be equal,  $d$ , and the middle gap to equal  $2d$ . The results of further generalizations of the geometry should be obvious and qualitatively minor. We label the upper ridge segment with the index 1 and the southern segment with index 2.

#### a. Theory

The principal new addition to the problem is that there are now *two* ridge constants to determine,  $\Psi_1$  for the northern ridge and  $\Psi_2$  for the southern ridge. The problem development follows the analysis of section 2 very closely. Thus on each side of the ridge system:

$$\psi_R = e^{i(k(x-x_e)+\omega t)} \sum_{n=1} A_n \sin a_n(x-x_e) \sin n\pi y, \quad (3.1a)$$

$$\psi_L = e^{i(k(x-x_e)+\omega t)} \sum_{n=1} B_n \sin a_n x \sin n\pi y, \quad (3.1b)$$

where, again,  $k = 1/(2\omega)$ .

On  $x = x_r$  the streamfunction satisfies

$$\psi = \begin{cases} \Psi_2 \frac{y}{d}, & 0 \leq y \leq d \\ \Psi_2, & d \leq y \leq \frac{1}{2} - d \\ \Psi_2 + \frac{(y - 1/2 + d)}{2d}(\Psi_1 - \Psi_2), & \frac{1}{2} - d \leq y \leq \frac{1}{2} + d \\ \Psi_1, & \frac{1}{2} + d \leq y \leq 1 - d \\ \Psi_1 \frac{(1-y)}{d}, & 1 - d \leq y \leq 1. \end{cases} \quad (3.2)$$

Should  $\Psi_1$  differ from  $\Psi_2$  there would be flow through the central gap for the mode. On the other hand,

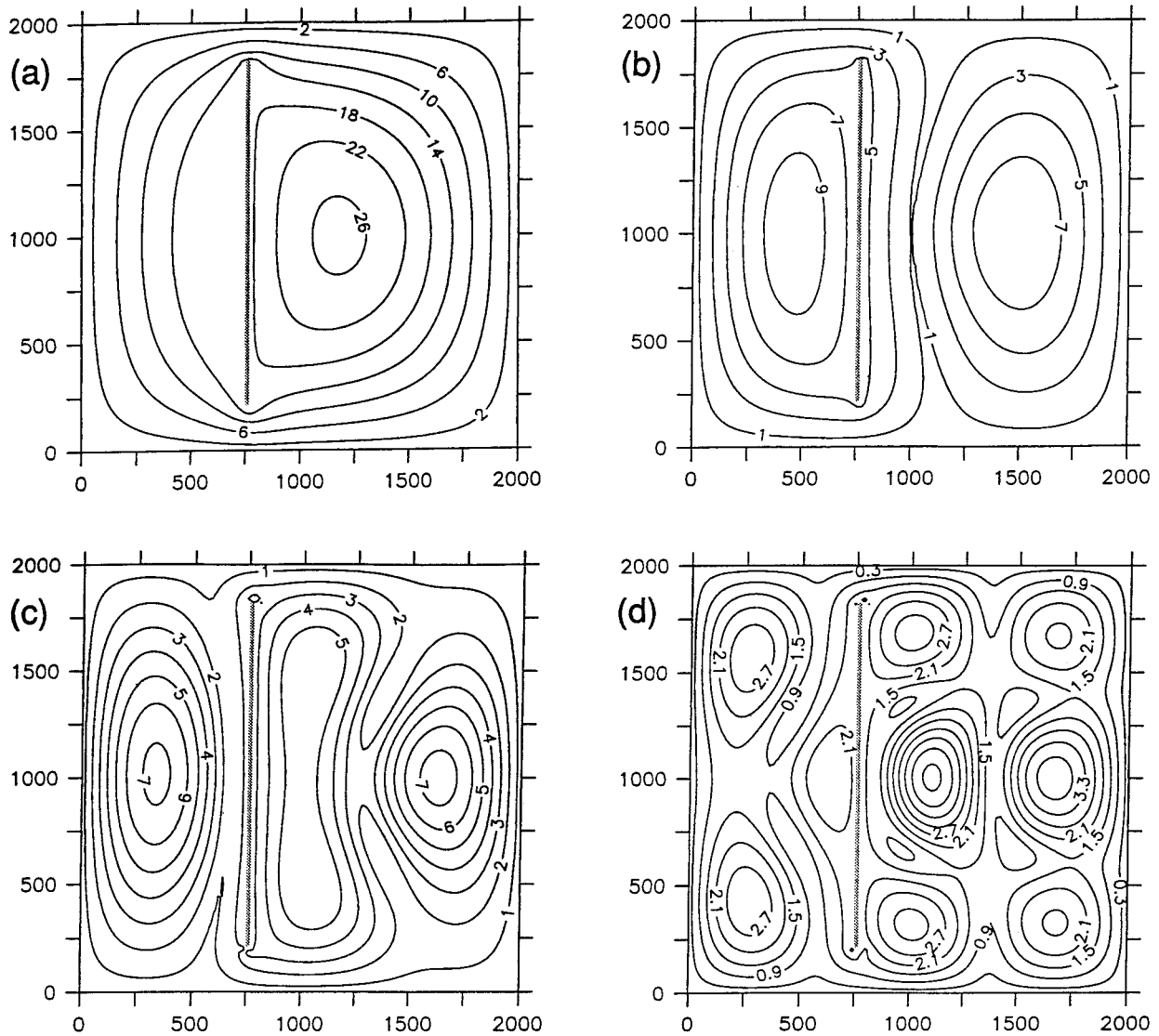


FIG. 6. Streamfunction variance from the model for forcing frequencies (a) 0.104, (b) 0.070, (c) 0.050, (d) 0.036, corresponding to the theoretical membrane functions in Figs. 3a–d.

if they should be equal, there would be no flow through the gap.

The analysis is now straightforward. One relation between the coefficients  $A_n$  and  $B_n$  follows from equating

both (3.1a) and (3.1b) to (3.2) on  $x = x_i$ . Then the integral constraint (2.11) is applied *on each segment separately*. A little algebra then yields the following equations for  $\Psi_1$  and  $\Psi_2$ :

$$\sum_{n=1} \frac{a_n \sin a_n x_e \sin n \pi d}{dn^3 \pi^3 \sin a_n x_i \sin a_n x_{ie}} \left\{ \cos n \pi d [(-1)^n - 1] + 2 \sin \frac{n \pi}{2} \sin n \pi d \right\} \times \left[ \Psi_2 - (-1)^n \Psi_1 + (\Psi_1 - \Psi_2) \cos \frac{n \pi}{2} \right] = 0, \tag{3.3a}$$

$$\sum_{n=1} \frac{a_n \sin a_n x_e \sin n \pi d}{dn^3 \pi^3 \sin a_n x_i \sin a_n x_{ie}} \left\{ \cos n \pi d [(-1)^n + 1] - 2 \cos \frac{n \pi}{2} \cos n \pi d \right\} \times \left[ \Psi_2 - (-1)^n \Psi_1 + (\Psi_1 - \Psi_2) \cos \frac{n \pi}{2} \right] = 0, \tag{3.3b}$$

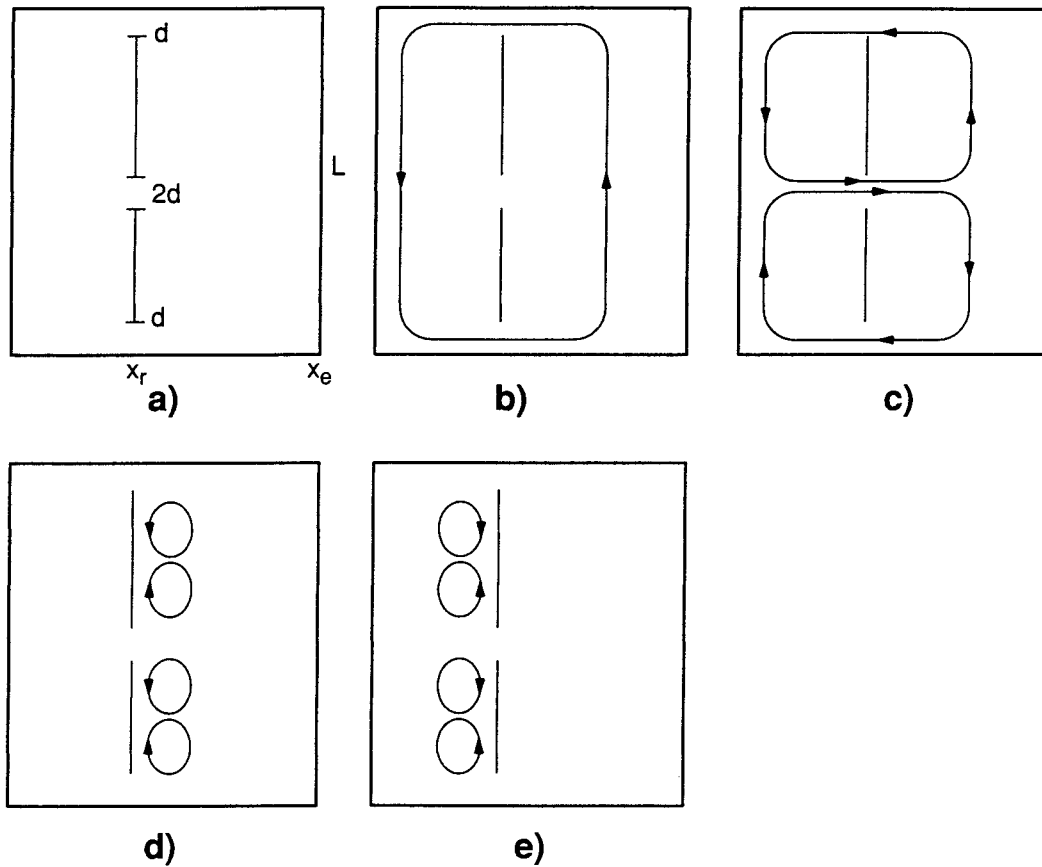


FIG. 7. (a) The configuration of a ridge with a central gap as well as gaps at its termini. (b) Schematic of the “odd” mode structure nearly identical to that of section 2. Note that there is no flow through the center gap. (c) Schematic of a class of higher meridional modes that are even  $n$  modes and maintain a substantial flow through the gap. (d) and (e) Schematics of higher  $n$  even modes that are limited to one or the other of the subbasins.

where again  $x_{te} = x_e - x_t$ .

Consider first (3.3b). For odd  $n$  the braced cosine functions are zero, so only even  $n = 2m$  with  $m$  an integer needs to be considered. In that case, (3.3b) becomes

$$\sum_{m=1} \frac{\hat{a}_m \sin(\hat{a}_m 2x_e) \sin 2m\pi d}{dm^3 \pi^3 \sin \hat{a}_m 2x_t \sin \hat{a}_m 2x_{te}} [(-1)^m - 1]^2 \times (\Psi_1 - \Psi_2) = 0, \tag{3.4a}$$

where

$$\hat{a}_m = \left[ \frac{1}{4\hat{\omega}^2} - m^2\pi^2 \right]^{1/2},$$

$$\hat{\omega} = 2\omega.$$

For (3.3a) all the terms for  $n$  even are zero and the sum extends only over  $n$  odd, yielding

$$\sum_{n \text{ odd}} \frac{a_n \sin a_n x_e \sin n\pi d}{dn^3 \pi^3 \sin a_n x_t \sin a_n x_{te}} [\cos n\pi d + (-1)^{(n+1)/2} \sin n\pi d] \times (\Psi_1 + \Psi_2) = 0. \tag{3.4b}$$

The interpretation of these results follows easily. Equation (3.4a) should be compared with (2.12). It follows that (3.4a) is the dispersion relation for a basin that has an aspect ratio in which the zonal to meridional lengths have doubled and the nondimensional gap widths have doubled, but otherwise the dispersion relation is identical. This corresponds to modes exactly as those in section 2, but whose scale is half the total meridional scale and identically folded over and reflected into the lower half of the basin. That is, they represent a second meridional harmonic mode as illustrated schematically in Fig. 7c. The frequency  $\omega = \hat{\omega}/2$ . The frequency is reduced by  $1/2$  because the characteristic length scale of the mode is half of the basin, that is,  $L/2$ . To satisfy (3.4b) it follows that for this mode  $\Psi_1 = -\Psi_2$ , so there is a flux through the central gap as indicated in Fig. 7c. Qualitatively, this is merely the mode of section 2 reflected around the midpoint of the basin. This mode is constructed of the Fourier modes  $n = 2m$  for  $m$  odd and consists of the Fourier  $\sin n\pi y$  modes for  $n = 2, 6, 10, \dots$ .

On the other hand, (3.4b) yields a mode constructed

from the solution of the Fourier sine series with  $n = 1, 3, 5, \dots$  terms. To satisfy (3.4a) we must now have  $\Psi_1 = \Psi_2$  so that there is no flow through the center gap for these “odd” modes. For these modes the central gap plays very little role at all, and the mode is nearly identical to the odd modes found in section 2. There is a slight difference associated with the second cosine function within the braces in (3.4b), which results from the fact that the circulation integral extends a distance  $2d$  less, because of the middle gap, than in the case of section 2 when the gap is absent. The difference is minor. These modes correspond then to the modes already found, and are indicated schematically in Fig. 7b.

Finally, solutions constructed of the Fourier sine modes with  $n = 4, 8, 12, 16, \dots$ , which are the Fourier modes unused in the construction of the two mode types discussed above, automatically satisfy the circulation condition on *each* ridge segment. They are indicated schematically in Figs. 7d and 7e and are purely subbasin modes.

The presence of the gap in the middle of the ridge has allowed some of the normal modes, previously confined to one or the other of the subbasins, to now become full-basin modes. As more gaps are opened in the ridge, higher modal structures, including some of those in Figs. 7d and 7e, will become full-basin modes. It is remarkable how the opening of a slight gap in the ridge, allowing the communication of the pressure signal from one subbasin to the other, can so dramatically alter the structural character of the normal modes.

#### b. Numerical model results

The role of the gap in facilitating the communication between basins at frequencies close to the resonant frequency for  $n = 2$  in one of the subbasins is now demonstrated. The streamfunction variance for two model calculations is shown in Fig. 8. The model is forced over a small region in the southern part of the eastern subbasin at a frequency  $\omega = 0.06165$ , the resonant frequency for the  $n = 2, m = 1$  mode for the eastern subbasin. As expected, the eastern subbasin is readily excited. In the absence of a gap in the meridional island, all of the variance is trapped in the eastern basin (Fig. 8a). Limiting the communication between basins to the northern and southern gaps does not allow for the propagation of any even mode variance from one subbasin to the other. This is because the island constant requires that the flow through one gap be equal and opposite to the flow through the other gap, thus allowing only information that is antisymmetric about the midlatitude to be communicated through the gaps. The meridional island is very effective at isolating adjacent subbasins to even modes of variability and, as previously demonstrated, is quite ineffective at isolating adjacent basins to odd modes of variability.

The introduction of a small gap at the middle of the basin eliminates this constraint because the streamfunction constant on the two islands need not be the same,

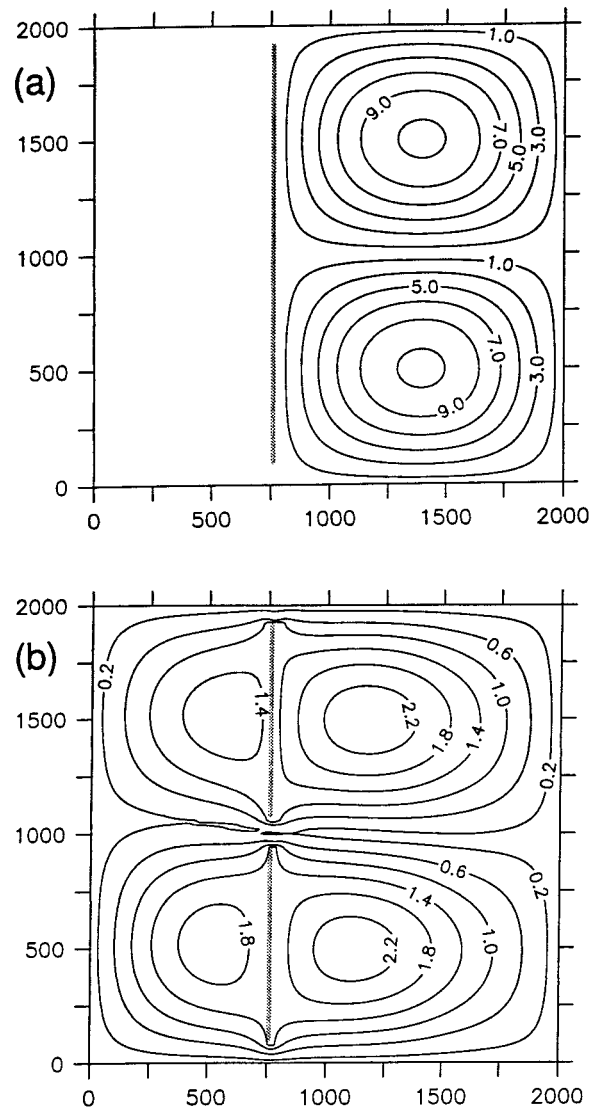


FIG. 8. Streamfunction variance from the model with forcing at the resonant frequency for the  $n = 2, m = 1$  eastern subbasin mode ( $\omega = 0.06165$ ) with (a) a single meridional ridge and (b) two meridional ridge segments separated by a narrow gap at the midlatitude of the basin.

as discussed above. The resulting variance shows that both subbasins are excited with strong flows through all three gaps, in qualitative agreement with the circulation sketched in Fig. 7c. There are of course many possible combinations of subbasin modes and island segments that could be explored. We show this simplest extension from the single island case to demonstrate the importance of the island circulation integral and the island constant in controlling the communication between adjacent basins and the structure of the flow far from the island.

#### 4. Zonal barrier

We now consider the situation illustrated in Fig. 9. The basin is once more nearly divided into two subbasins by

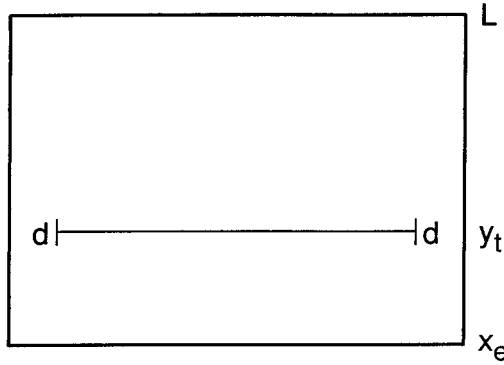


FIG. 9. The configuration for the case of a zonal barrier. The barrier is located at  $y = y_t$  and the two subbasins now communicate through narrow gaps located at the zonal extremities of the barrier. Again, the gaps have width  $d \ll L$ .

a barrier but this time the barrier lies along a latitude circle and is located at  $y = y_t$ . Once again the gaps at the ends are small,  $d \ll L$ . The new orientation of the barrier leads to important changes in the modal problem.

a. Theory

From a technical point of view it follows that although the form of the solution (2.2) is still a useful representation of the solution, the function  $\phi$  can no longer be constant on the barrier. Indeed,  $\phi$  must be chosen to cancel the  $x$  variation of the traveling plane wave on the ridge so that the streamfunction there remains only a function of time and not of  $x$ . That is, on the ridge

$$\phi = \Psi_l e^{-ikx}, \tag{4.1}$$

where once again  $k = 1/(2\omega)$ . Related to this technical alteration is the loss of symmetry associated with the membrane function  $\phi$ . It is no longer a simple odd-or-even function of  $x$  around the midlongitude point of the basin. It follows from this that the separation into full-basin modes and subbasin modes will no longer obtain so that now *all* modes will be manifest on either side

of the basin. There is no solution for which both  $\psi_l = 0$  and  $\int_d^{1-d} \partial\psi/\partial y dx$  is zero on one side of the barrier. Nevertheless there will be, as shown below, a tendency for some modes to be more energetic in one or the other of the subbasins depending on the frequency of the mode.

The analysis is analogous to the case of the meridional barrier. The solution for  $\phi$  is represented in terms of Fourier representation in  $x$ ; that is,

$$\begin{aligned} \phi &= \phi^N \\ &= \sum_{m=1} A_m \sin a_m (1 - y) \sin m\pi x, \quad y \geq y_t, \end{aligned} \tag{4.2a}$$

$$\phi = \phi^S = \sum_{m=1} B_m \sin a_m y \sin m\pi x, \quad y \leq y_t. \tag{4.2b}$$

We have chosen  $x_e = 1$  for simplicity. As before,

$$a_m = (k^2 - m^2 \pi^2)^{1/2}. \tag{4.3}$$

Also as before, we assume that on the barrier  $\psi = \Psi_l$  and falls linearly to zero at the boundary of the basin. This implies that

$$\phi = \Psi_l e^{-ikx} \begin{cases} x/d, & 0 \leq x \leq d \\ 1, & d \leq x \leq 1 - d \\ (1 - x)/d, & 1 - d \leq x \leq 1, \end{cases} \tag{4.4}$$

which should be compared with (2.8). Note again that in (4.4)  $d$  is the nondimensional gap width (scaled by  $L$ ).

The circulation integral constraint is now

$$\int_d^{1-d} \frac{\partial\psi}{\partial y}(x, y_{t+}) dx = \int_d^{1-d} \frac{\partial\psi}{\partial y}(x, y_{t-}) dx. \tag{4.5}$$

The satisfaction of (4.4) and (4.5) yields the relation between the set  $(A_m, B_m)$  and the island constant  $\Psi_l$ , and is given in appendix A. The circulation integral (4.5) then yields the dispersion relation for the normal modes. After some algebra,

$$\Psi_l \sum_{m=1} \frac{\Gamma_m \sin a_m}{a_m \sin a_m y_t \sin a_m (1 - y_t)} = 0, \tag{4.6a}$$

where

$$\begin{aligned} \Gamma_m &= \frac{2m\pi \sin 2m\pi d}{da_m^4} [a_m^2 + (m^2 \pi^2 + 3k^2)(-1)^m \cos k(1 - d)] \\ &+ \frac{4k}{da_m^4} [2m^2 \pi^2 \cos^2 m\pi d - (m^2 \pi^2 + k^2) \sin^2 m\pi d] (-1)^m \sin k(1 - 2d) \\ &+ \frac{8km^2 \pi^2 \cos m\pi d}{da_m^4} [\sin kd - (-1)^m \sin k(1 - d)] - \frac{8k^2 m\pi \sin m\pi d}{da_m^4} [\cos kd + (-1)^m \cos k(1 - d)]. \end{aligned} \tag{4.6b}$$

The complexity of this dispersion relation, in contrast to that of the meridional barrier, is directly re-

lated to the structure of the membrane function given in appendix A, which has to cancel the  $x$  variation in

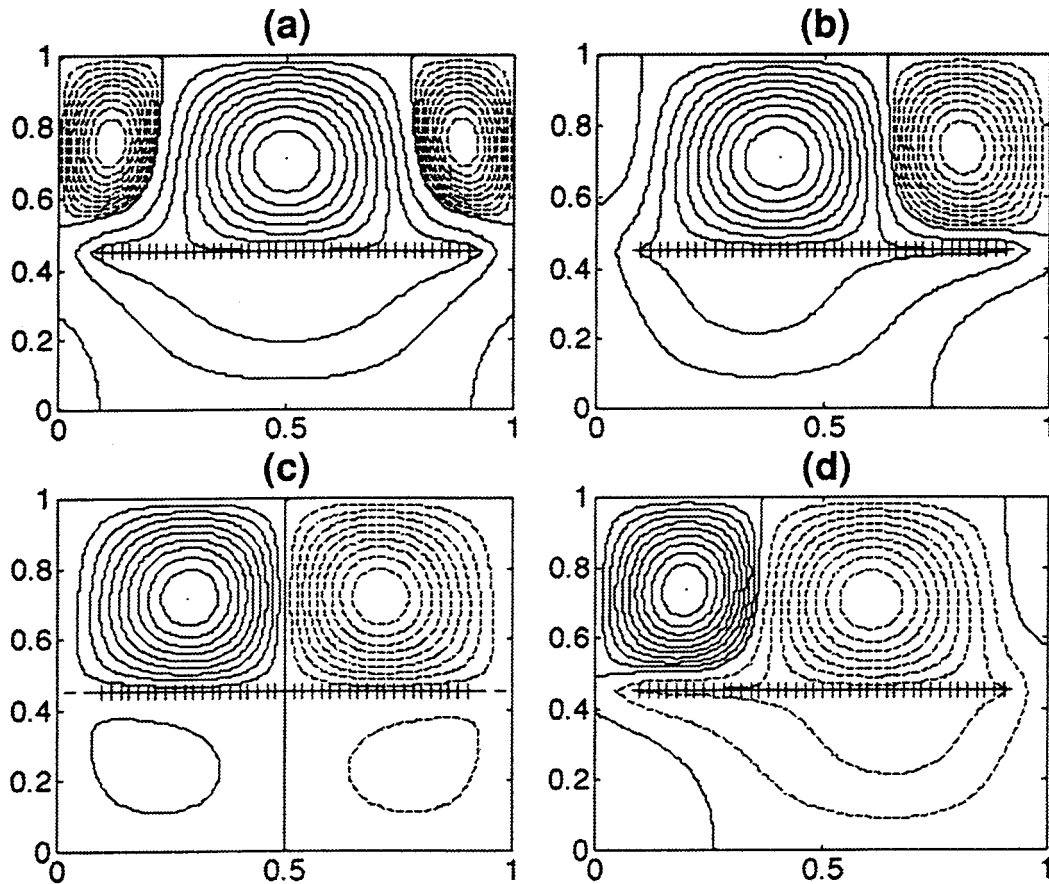


FIG. 10. The gravest normal mode for the zonal barrier,  $\omega = 0.0792$ . The streamfunction is shown at (a)  $\omega t = 0$ , (b)  $\omega t = \pi/4$ , (c)  $\omega t = \pi/2$ , and (d)  $\omega t = 3\pi/4$ . For this case  $d = 0.1$  and  $y_b = 0.45$ .

the traveling wave component of the solution along the ridge.

In spite of the complexity of (4.6) it is fairly easy to find the solutions for  $\omega$  numerically. This is rendered even easier when we discover that the normal-mode frequencies are always *very close although not equal to the normal-mode frequencies for each of the subbasins*. For example, Fig. 10 shows the normal mode with the largest frequency for the case  $y_b = 0.45$ . The mode is shown at four phases during the oscillation, that is, at  $\omega t = 0, \pi/4, \pi/2$ , and  $3\pi/4$ . The mode consists of a traveling set of vortical structures that are dominant in the northern subbasin. However, it is clear that there is significant motion in the lower subbasin. As mentioned earlier, the separation of the normal modes into full-basin and subbasin modes, as occurred for the meridional barrier, no longer is apt for the zonal case. The frequency of this normal mode (scaled by  $\beta L$ ) is  $\omega = 0.07915$  and this should be compared to the Rossby normal-mode frequency for a basin consisting only of the *northern* subbasin. That frequency is  $\omega = 0.0767$  for  $m = 1, n = 1$ . The proximity of these frequencies makes the dominance of the mode in the northern subbasin intuitive. The normal mode with the *next* largest

frequency is found at  $\omega = 0.06642$  and is shown in Fig. 11. In this case the mode has its principal expression in the southern subbasin. The frequency of the gravest mode for a basin with the dimensions of the southern subbasin would be  $\omega = 0.0653$  if the gaps between the two subbasins were completely closed.

For modes with lower frequencies, the normal-mode frequencies become more densely spaced, and the separation between northern and southern mode types is less pronounced. For example, Fig. 12 shows the case for  $\omega = 0.0436$ . This mode has a strong expression in both subbasins. Of course, for the lower frequency modes the  $x$  wavenumber of the traveling wave component increases and the scale in  $x$  decreases inversely.

If we examine the snapshots of the modal structure, it is clear that there are points during the oscillation when the modes leak less into the other subbasin than at other times. This is connected to the march of the value of the streamfunction on the barrier. For the gravest mode, shown in Fig. 10, we have plotted the streamfunction from the solutions (2.2) and (4.2) along the latitude of the barrier at  $y = y_b$ , as shown in Fig. 13. (This also serves as a check on how well our truncated Fourier series, in which 50 modes are retained, is able

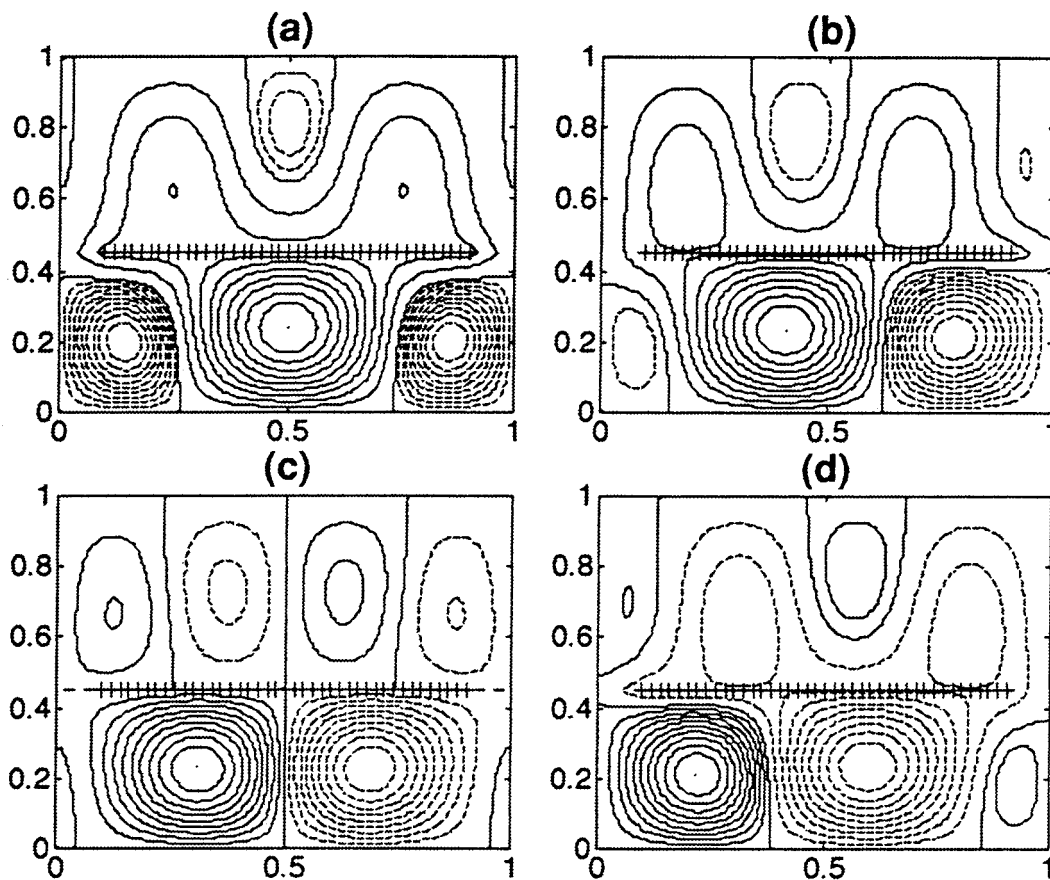


FIG. 11. As in Fig. 10 except that  $\omega = 0.066\ 42$ .

to represent the solution.) We see that the island constant oscillates harmonically, and at the phase  $\omega = \pi/2$  the constant falls to zero. At this moment there is no flow through the gap. The two subbasins are essentially isolated, and the dominant signal is in the northern basin. At other points in the cycle, for example, at  $\omega t = 3\pi/4$ , there is a strong variation of the streamfunction across the gaps. This leads to substantial flow through the gaps, and communication is established between the two subbasins as shown in Figs. 13a,b,d.

Thus both for the case of the meridional barrier, as well as for the zonal barrier, Rossby normal modes that involve the full basin are obtained. In the zonal barrier case there is no separation between full-basin modes and subbasin modes as was the case for the meridional barrier studied in section 2. Furthermore, the frequencies for the zonal case are closer, for all modes, to the normal-mode frequencies for the separate subbasins than is the case for the meridional barrier. We understand this to be a reflection of the stronger inhibition of meridional motion for the case of the zonal barrier and consequently a lesser restoring agency due to the  $\beta$  effect. Nevertheless, even in this case, the energy leaks substantially from one subbasin to the other, and this is especially true at low frequencies.

*b. Numerical model results*

The structure of the variability excited for the case of a zonal island has also been investigated numerically. Two snapshots of the streamfunction in the model forced with frequency  $\omega = 0.079\ 15$  at phase 0 and  $\pi/2$  are shown in Fig. 14. The general character of the circulation predicted by the theory is reproduced in the model, although there are some differences. The strength of the interbasin exchange is larger in the model and, as a result, the strengths of the lows in the northern half of the basin are slightly reduced at zero phase. At phase  $\pi/2$  there is no net circulation around the island, in agreement with the theory. However, the multidirectional flow through each of the gaps does not agree with the unidirectional flow assumed in the theory. This difference may be responsible for the enhanced circulation around the island found in the model.

At the frequency of the next mode,  $\omega = 0.066\ 42$ , the model produces a circulation similar to that predicted by theory (Fig. 15). The wavelength and sense of the recirculations is the same as predicted by the theory; however, once again there is a stronger interbasin exchange and circulation around the island in the model. Reducing the gap width below  $d = 0.1$  reduces

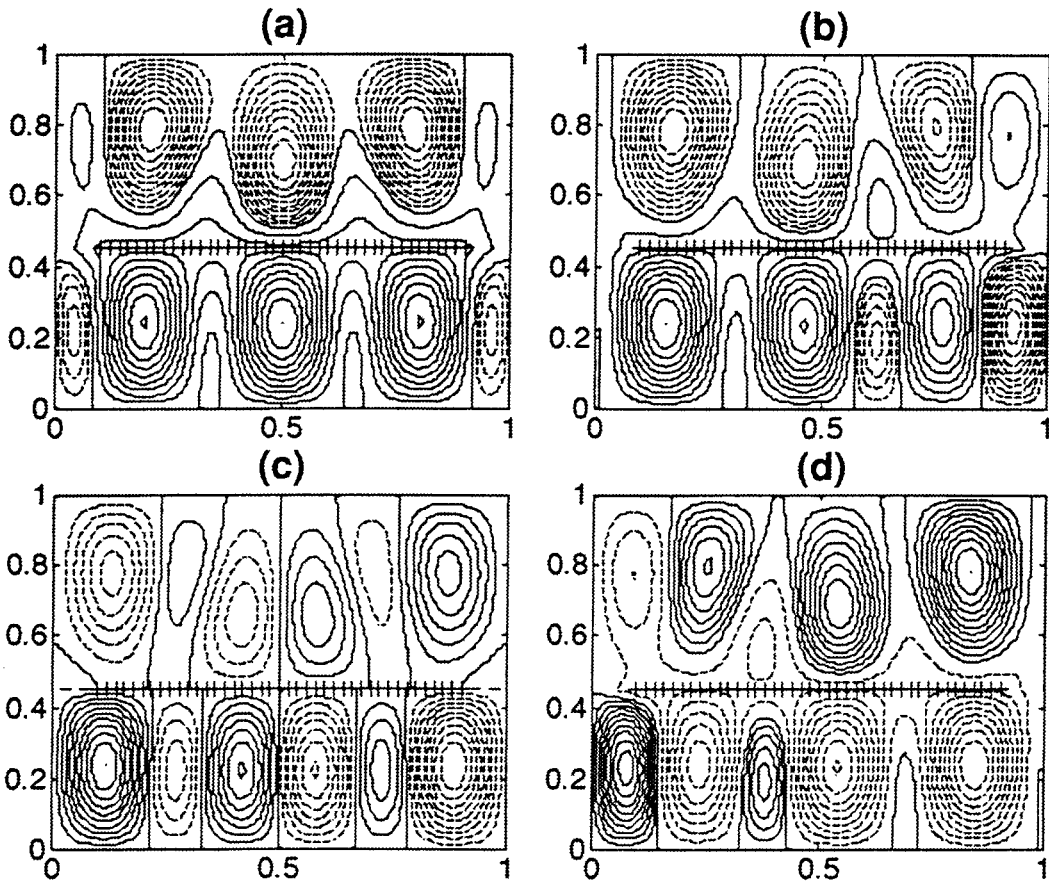


FIG. 12. As in Fig. 10 except that  $\omega = 0.0436$ .

the multidirectional flow through the gaps and the net circulation around the island, bringing the model results in closer agreement with the theory, which assumes  $d \ll 1$ .

**5. Discussion**

We have found full-basin Rossby normal modes in basins nearly cleaved in two by a barrier allowing communication between the subbasins only through a small number of narrow gaps. This rather surprising result is a direct consequence of the application of the circulation integral around the barrier "island," which requires, generally, a strong circulation on each side of the barrier unless special symmetry conditions are met by the modes. The presence of the gaps allows a strong pressure signal to link each side of the basin to the other. We believe this result has important consequences for the variability of the abyssal ocean. This result should be compared with the study of Anderson and Killworth (1977), who examined the role of a (small) ridge extending the entire basin length in which only the sub-basin modes obtained.

In the case of a meridional barrier, which is our crude model of a midocean ridge, the frequencies of the full-basin normal modes are very close to the frequencies of the basin modes in the absence of the barrier. Sub-basin modes, in which the motion is limited to one of the two subbasins, only occur for those symmetries that allow the subbasin mode to satisfy the circulation in-

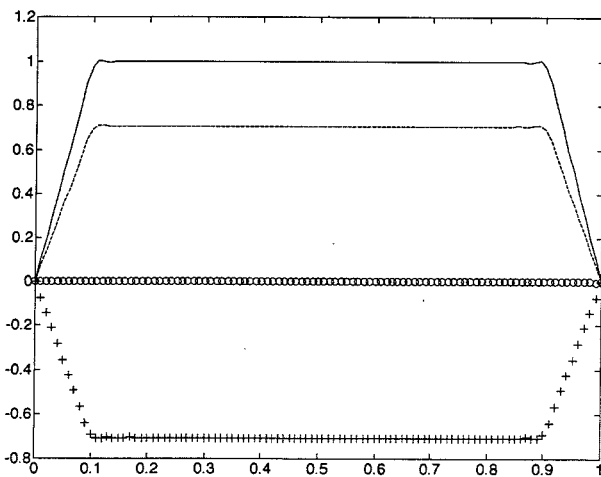


FIG. 13. The streamfunction along the line  $y = 0.5$ , at the four phases of the oscillation shown in Fig. 10.

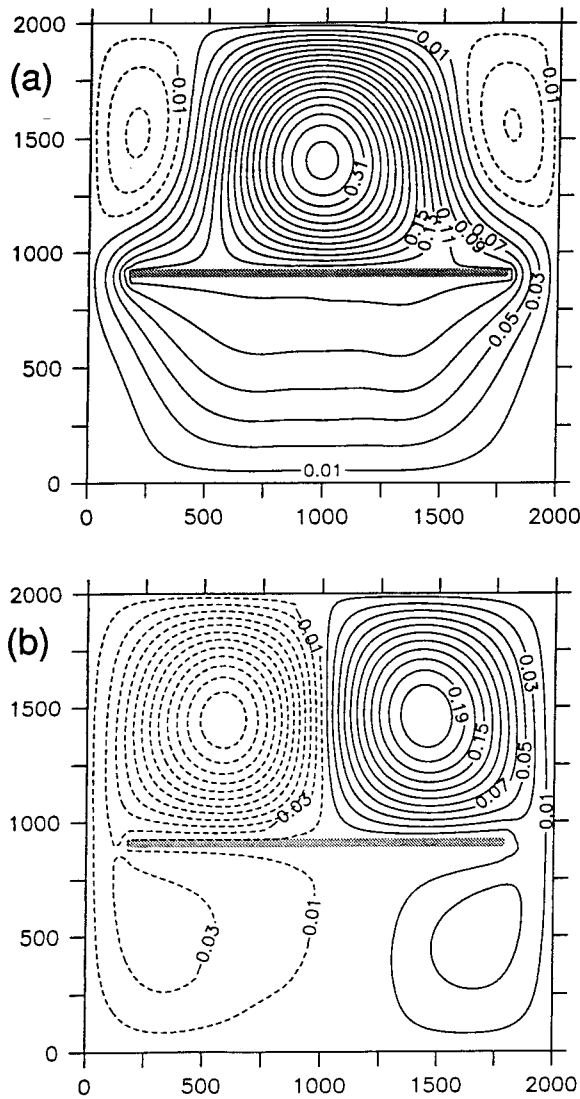


FIG. 14. Streamfunction from the model for the zonal island case with forcing frequency 0.079 15 at phase (a) 0, (b)  $\pi/2$ . These are to be compared with the theoretical circulation in Figs. 10a and 10c.

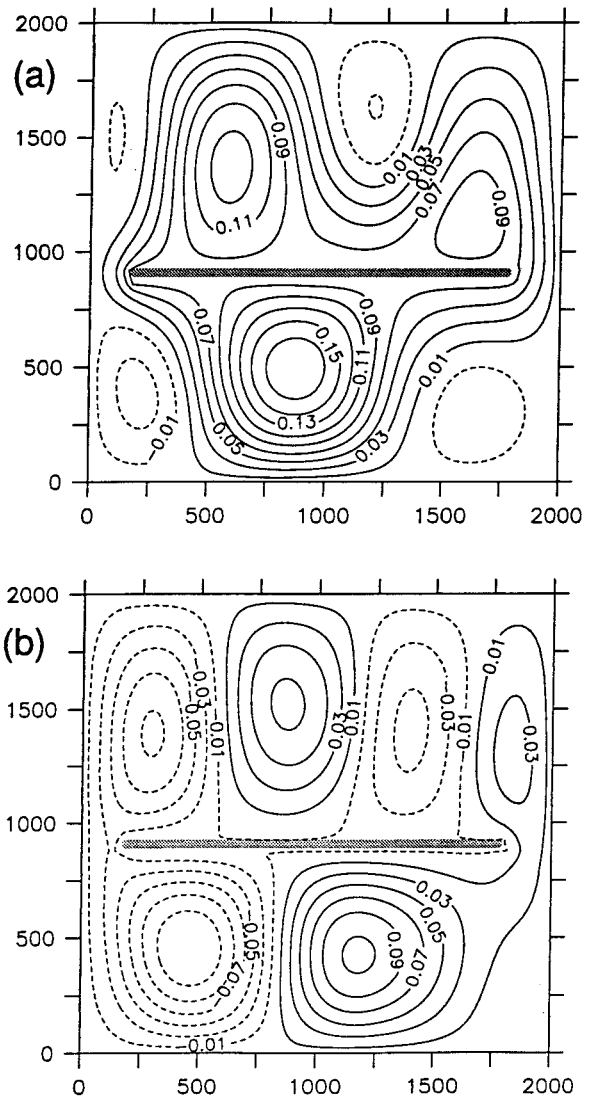


FIG. 15. Streamfunction from the model for the zonal island case with forcing frequency 0.066 42 at phase (a) 0, (b)  $\pi/2$ . These are to be compared with the theoretical circulation in Figs. 11a and 11c.

tegral constraint alone. For example, with gaps at each end of the basin, modes with odd symmetry around the midlatitude of the basin would satisfy the integral constraint (2.11) for the subbasin modes. We have shown then how increasing the number of gaps transforms some of the isolated subbasin modes into full-basin modes.

Each additional piercing of the ridge requires a higher along-ridge wavenumber in the adjoining basin to satisfy the integral constraint yielding a full-basin mode with a higher meridional mode number.

Note that it follows that were the basin nearly divided by a *peninsula*, that is, a barrier attached to, say, the northern boundary of the basin, *only* subbasin modes would be possible as the sole remaining gap would be ineffective in allowing a mass flux between the two

subbasins. This coincides with the requirement that  $\psi$  be zero on the peninsula (since it is attached to the outer boundary of the basin) so that no net flow occurs between the tip of the peninsula and the southern boundary of the basin. The occurrence of a gap at the northern end of the island allows the set of basin-scale normal modes discussed in section 2 to spring into being.

As shown in PPSH, when the gap becomes narrow enough so that frictional forces become large enough to support a significant pressure drop across the gap, the isolated barrier can metamorphose, dynamically, into a peninsula. As shown here, this will have a dramatic effect on the communication of natural variability from one sector of the basin to another. In PPSH we showed that the gap had to become increasingly narrow in latitudinal extent the narrower the barrier became in

longitudinal extent. It will be extremely interesting to test for the critical width of the gap that eliminates full-basin normal modes in a laboratory experiment of the type reported in PPSH. Such experiments are planned for the future. For the narrow ridgelike barriers described here, we anticipate that the gaps would have to be considerably narrower than a Munk boundary layer thickness to eliminate the full-basin modes.

The zonal barrier discussed in section 3 possesses only full-basin modes, although the nature of the normal mode is such that during different phases of the oscillation the normal mode briefly resembles the subbasin mode of one of the two subbasins. In this case the normal modes have frequencies close to the normal-mode frequencies of each of the subbasins.

The excellent agreement between the numerical results, in which the normal modes are found by a frequency scan for resonance of the forced problem, and the analytical normal-mode calculation encourages us to believe that the normal modes might be easily excited in both the laboratory and the natural ocean. The implications of the latter possibility would be quite striking if true. Spatially localized forcing due to a wide variety of causes, within the frequency band of the normal modes, could be expected then to yield full-basin variability in spite of the apparent barriers to communication between the subbasins in the abyssal oceans.

In future work we intend to study the effects of non-linearity, in particular the role of eddy shedding at the barrier termini, on the basin normal modes and on the general problem of interbasin communication of variability. The interaction of the normal modes with mean flows and instabilities also deserves further and detailed study. Naturally, given the results already shown in Fig. 1, we intend to extend our results to baroclinic models of the circulation. The geometry of our model itself is highly idealized, and it will be of interest in examining the role that more realistic representations of the topography will play in the dynamics, especially in examining the impedance of the flow between adjacent subbasins. Both the topography of the ridge segment, or island, and the bottom topography of the straits represented here by simple gaps in the barrier, are in reality far more complex and present challenges for future work.

*Acknowledgments.* This research was supported in part by National Science Foundation Grants OCE 93-01845 (JP) and OCE 95-31874 (MS).

## APPENDIX A

### Fourier Coefficients for a Zonal Ridge

The condition (4.4) yields for the Fourier coefficients in (4.2)

$$A_m \sin a_m(1 - y_i) = \Psi_l \frac{2im\pi x}{\omega da_m^4} [(1 + (-1)^m e^{-ik}) - \cos m\pi d(e^{-ikd} + (-1)^m e^{-ik(1-d)})] + 2\Psi_l \left[ \frac{m^2\pi^2 + k^2}{a_m^4} \right] \frac{\sin m\pi d}{d} [e^{-ikd} - (-1)^m e^{-ik(1-d)}], \quad (\text{A.1})$$

while

$$B_m = A_m \frac{\sin a_m(1 - y_i)}{\sin a_m y_i}. \quad (\text{A.2})$$

## APPENDIX B

### The Numerical Model Equations

The MICOM solves the primitive equations in isopycnal coordinates, which are included here for reference. The horizontal momentum equation, with no cross-isopycnal mass flux is given by

$$\frac{\partial \mathbf{v}}{\partial t} + \nabla \frac{\mathbf{v}^2}{2} + (\zeta + f)\mathbf{k} \times \mathbf{v} + \nabla_\alpha M = -g \frac{\tau}{\Delta p} + (\Delta p)^{-1} \nabla \cdot (A \Delta p \nabla \mathbf{v}) - c_D \mathbf{v}, \quad (\text{B.1})$$

where  $\mathbf{v} = (u, v)$  is the horizontal velocity vector,  $p$  is the pressure,  $\mathbf{k}$  is the vertical unit vector,  $\zeta = \partial v / \partial x - \partial u / \partial y$  is the relative vorticity,  $M = gz + p\alpha$  is the Montgomery potential,  $\alpha$  is the specific volume of the layer (constant),  $\Delta p$  is the pressure thickness of the layer, and  $A$  is an eddy viscosity coefficient. The  $\beta$ -plane approximation is used here, with  $f = f_0 + \beta y$ . The model is forced with a wind stress of strength  $\tau$ . There is no explicit subgrid-scale mixing in the model ( $A = C_D = 0$ ). The standard lateral boundary conditions are no-slip for momentum and no flux for density. However, for the linear calculations reported in this paper, the lateral viscosity is identically zero so that free-slip and no-slip boundary conditions give identical results. We have also repeated many of the central calculations of the paper with viscosities of  $O(100 \text{ m}^2 \text{ s}^{-1})$  and find very similar results using both free-slip and no-slip boundary conditions.

In the absence of cross-isopycnal mass fluxes, the continuity equation is represented as a prognostic equation for the layer thickness  $\Delta p$ ,

$$\frac{\partial \Delta p}{\partial t} + \nabla \cdot (\mathbf{v} \Delta p) = 0. \quad (\text{B.2})$$

For the present application with no surface buoyancy forcing, no cross-isopycnal mass flux, and uniform temperature and salinity within each layer, the conservation equations for these thermodynamic variables maintain constant values within each layer and thus are not presented here. The complete model equations and details about the numerical methods used to integrate the equations, can be found in Bleck et al. (1992).

## REFERENCES

- Anderson, D. L. T., and P. D. Killworth, 1977: Spin-up of a stratified ocean, with topography. *Deep-Sea Res.*, **24**, 709–732.
- Bleck, R., C. Rooth, D. Hu, and L. T. Smith, 1992: Salinity-driven thermocline transients in a wind- and thermohaline-forced isopycnal coordinate model of the North Atlantic. *J. Phys. Oceanogr.*, **22**, 1486–1505.
- Flierl, G. R., 1977: Simple applications of McWilliams's "A note on a consistent quasi-geostrophic model in a multiply connected domain." *Dyn. Atmos. Oceans*, **1**, 443–454.
- Godfrey, J. S., 1989: A Sverdrup model of the depth-integrated flow for the world ocean allowing for island circulations. *Geophys. Astrophys. Fluid Dyn.*, **45**, 89–112.
- Pedlosky J., 1987: *Geophysical Fluid Dynamics*. Springer-Verlag, 710 pp.
- , L. J. Pratt, M. A. Spall, and K. R. Helfrich, 1997: Circulation around islands and ridges. *J. Mar. Res.*, **55**, 1199–1251.